Use of the Finite Element Method for the Modeling of Multi-Layered Power/Ground Planes with Small Features

Krishna Bharath[†], Jae Young Choi [‡] and Madhavan Swaminathan [§]
School of Electrical and Computer Engineering
Georgia Institute of Technology
Atlanta, GA 30332
Email: [†]kbharath@ece.gatech.edu, [‡]jaeyoung.choi@gatech.edu, [§]madhavan@ece.gatech.edu

Abstract

In this paper, a novel formulation for the modeling of multi-layer package power/ground planes has been proposed. The formulation is developed by first applying the finite element method (FEM) for a single plane-pair geometry, from which a SPICE-compatible equivalent circuit is extracted. Next, the admittance matrices obtained for individual plane-pairs are coupled together, to extend the technique, and to enable the modeling of multiple plane-pairs. This method, the mutli-layer finite element method (MFEM), uses an adaptive triangular mesh. This enables MFEM to capture the effects of small geometrical features that can affect the frequency response, with only a modest increase in computational cost as compared to methods that use regular square meshes. MFEM is able to correctly model the effect of apertures or voids in the planes, which cause vertical coupling of energy. Several examples have been shown to illustrate the efficacy of the method for both single and multiple plane-pair geometries.

I. Introduction

The power delivery network (PDN) of packaged mixed-signal electronic systems is becoming ever more complex as increasing number of components are integrated. Due to the various types of components in the system, multiple power supplies are typically required. These power supplies are designed as alternating layers of power and ground planes, with signal lines routed in layers that are sandwiched in between. These power/ground planes prevent signal lines on different layers from getting coupled to each other. A schematic illustration of a package for a multi-chip module is shown in Figure 1. To provide DC isolation to the different supply voltages, as well as to provide via anti-pads and to route signal lines, apertures and holes are created in the solid power/ground planes. These discontinuities in the power/ground planes can cause vertical coupling of energy. This is particularly critical in the context of simultaneous switching noise (SSN) or delta-I noise which can result in large fluctuations in supply voltage. These voltage fluctuations can propagate across the entire PDN causing signal integrity (SI) and power integrity (PI) problems [1], as well as electromagnetic interference (EMI) because of edge radiation. Therefore, an accurate and computationally efficient modeling of the PDN is critical to evaluate noise levels in mixed-signal systems.

The numerical solution of these problems using full-wave EM solvers is computationally intractable due to the large problem size. Generic commercial 3D-FEM techniques, while resulting in sparse systems, typically contain far too many unknowns. The method-of-moments(MoM)-based approaches

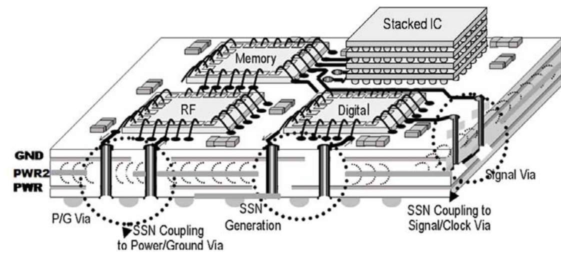

Fig. 1. Schematic of a multi-chip module.

result in systems which contain fewer unknowns, which, however, are dense. Thus, several techniques have been developed in literature for solving the multi-layered package PDN problem.

One solution that has been proposed is the multi-layer finite difference method (MFDM) [2]. MFDM is a finite difference-based technique that can solve power plane problems using square-meshes. This method creates a sparse and banded admittance matrix and provides an efficient computational complexity of $O(N^{1.5})$ [3]. However, the method suffers from using a rigid, square, grid. Typically, package PDNs are electrically large and also contain geometrically small features such as split planes and apertures. To capture very fine structures, the regular mesh becomes dense locally and globally, resulting in a large number of unknowns. This problem can be solved by using a non-uniform rectangular mesh, which is also not optimal in the modeling of arbitrary geometries, such as circular voids and via-holes. Hence, techniques using non-uniform triangular meshes have been proposed in literature for two layer geometries with circuit extraction for SPICE compatibility [4]. However, FEM applied to multilayer geometries has typically used hexahedral or tetrahedral meshes [5]. These meshes, being volumetric, require significantly larger number of unknowns, which in turn translates to an increase in computational cost.

The contribution of this paper is a method, the multi-layer finite element method (MFEM)[6], that applies a surface mesh. As only a surface mesh is required, this approach requires far fewer unknowns than a general 3D FEM-based solution. The mesh is based on Delaunay triangulation and is applied to each metal layer. The potential distribution on each plane pair is expanded in terms of pyramid basis functions. On simplification, the obtained matrix equation can be shown to represent an electrical network.

Authorized licensed use limited to: Georgia Institute of Technology. Downloaded on August 26, 2009 at 14:46 from IEEE Xplore. Restrictions apply.

The rest of this paper is organized as follows. The formulation for single plane-pair geometries is developed in Section II. The extension to multiple plane-pairs id discussed in Section III. Results for model to hardware correlation and comparison to other simulation tools are demonstrated in Section IV, followed by conclusions in Section V.

II. Single Plane-Pair: Formulation

An efficient approximation that can be employed for package power planes is that of a planar circuit [7]. A planar circuit is a microwave structure in which one of the three dimensions, say z, is much smaller than the wavelength. Under this condition, it can be assumed that the field is invariant along the z-direction. Hence, $\frac{\partial}{\partial z} = 0$ and the governing equation reduces to the scalar 2D-Helmholtz wave equation:

$$\left(\nabla^2 + k^2\right) \mathrm{u} = j\omega\mu d J_z,\ \nabla^2 = \left(\frac{\partial^2}{\partial x^2} + \frac{\partial^2}{\partial y^2}\right) \quad (1)$$

where ∇^2 is the transverse Laplace operator parallel to the planar structures, u is the voltage, d is the distance between the planes, k is the wave number, and J_z is the current density injected normally to the planes [8]. The open circuit at the boundary can be represented by a magnetic wall or Neumann boundary condition, which completes the problem formulation.

A. Basis Function

Using a standard finite-element approximation with triangular mesh elements and linear pyramid or "hat"-basis functions [9], the weak form of the PDE in Equation (1) is:

$$\sum_{j=1}^{N} \int\int_{\Omega} \left[\nabla\phi_j \cdot \nabla\phi_i + \omega^2\mu\varepsilon\phi_j\phi_i + j\omega\mu d J_z \phi_i\right] dxdy = 0 \quad (2)$$

where Ω is the problem domain. The triangular mesh and the hat function, ϕ are shown in Figure 2(a). The formulation of the matrix equation for 2D geometries is well known, and is reproduced here from [10]. For convenience, simplex coordinates $\{L_1, L_2, L_3\}$ have been used, which can be related to the Cartesian coordinates:

$$x = L_1 x_1 + L_2 x_2 + L_3 x_3 \quad (3)$$
$$y = L_1 y_1 + L_2 y_2 + L_3 y_3 \quad (4)$$
$$L_1 + L_2 + L_3 = 1 \quad (5)$$

The equations above can be solved to obtain:

$$\begin{aligned} L_i &= \frac{1}{2\triangle}\left(a_i + b_i x + c_i y\right) \quad (6)\\ a_i &= x_{i+1}y_{i+2} - x_{i+2}y_{i+1}\\ b_i &= y_{i+1} - y_{i-1}\\ c_i &= x_{i-1} - y_{i+1} \end{aligned}$$

and the subscripts are evaluated $(\text{modulo } 3) + 1$. $\triangle$ is the area of the triangle with vertices at points $(P1, P2, P3)$. Within the cell, the pyramid basis functions are identical to the simplex coordinates themselves.

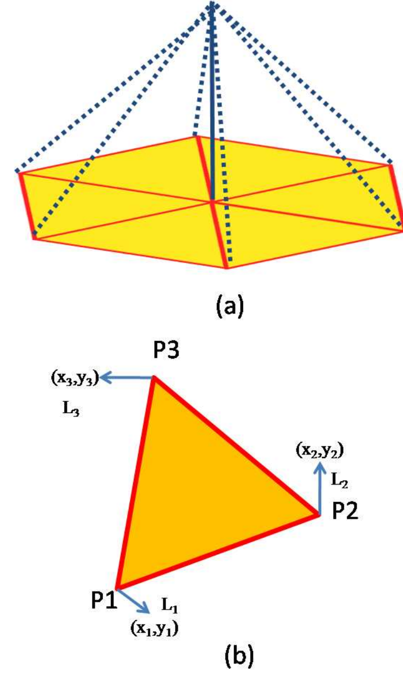

Fig. 2. (a) Triangular mesh and pyramid basis function (b) Cartesian and Simplex coordinates.

Hence, Equation (2) can be rewritten in matrix form as follows:

$$\left(\overline{\overline{\mathbf{K}}} + \overline{\overline{\mathbf{M}}}\right)\overline{\mathbf{U}} = \overline{\mathbf{F}} \quad (7)$$

where, $\overline{\overline{\mathbf{K}}}$ and $\overline{\overline{\mathbf{M}}}$ represent the stiffness and mass matrices, respectively, $\overline{\mathbf{U}}$ is the unknown potential, and $\overline{\mathbf{F}}$ contains the contributions from the current source excitation. The entries of $\overline{\overline{\mathbf{K}}}$, $\overline{\overline{\mathbf{M}}}$ and $\overline{\mathbf{F}}$ are:

$$\begin{aligned} k_{i,j} &= \int\int_{\Omega} \frac{j}{\omega\mu d}\nabla\phi_i \cdot \nabla\phi_j dxdy \quad (8)\\ m_{i,j} &= \int\int_{\Omega} \frac{-j\omega\varepsilon}{d}\phi_i\phi_j dxdy \quad (9)\\ f_i &= \int\int_{\Omega} J_z\phi_i dxdy \quad (10) \end{aligned}$$

The linear pyramid basis functions are equal to the simplex coordinates within the cell, i.e.

$$\phi_i(L_1, L_2, L_3) = L_i \quad (11)$$

Therefore,

$$\nabla\phi_i = \nabla L_i = \frac{1}{2\triangle}\left(\hat{x}b_i + \hat{y}c_i\right) \quad (12)$$

Substituting Equation 12 in Equation 8,

$$k_{i,j} = \frac{b_i b_j + c_i c_j}{4\triangle}\frac{j}{\omega\mu d} \quad (13)$$

The evaluation of the integral to obtain $m_{i,j}$ (Equation 9) and f_i (Equation 10) can be performed by transforming the coordinates from Cartesian to simplex using the Jacobian,

$$dxdy = dL_1 dL_2 \frac{\partial(x,y)}{\partial(L_1, L_2)} = 2\triangle dL_1 dL_2 \quad (14)$$

Authorized licensed use limited to: Georgia Institute of Technology. Downloaded on August 26, 2009 at 14:46 from IEEE Xplore. Restrictions apply.

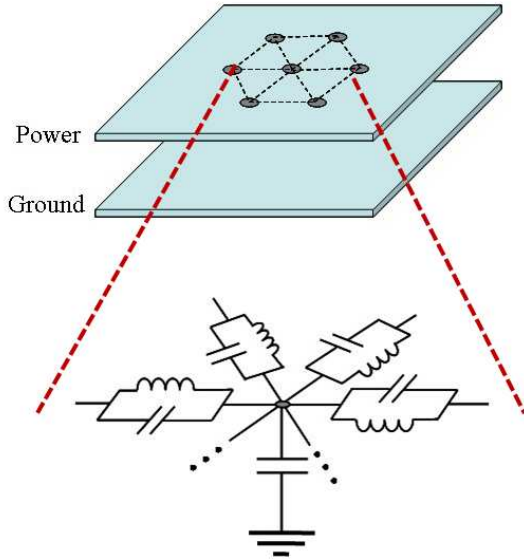

Fig. 3. Topology of equivalent circuit for single plane-pair structures.

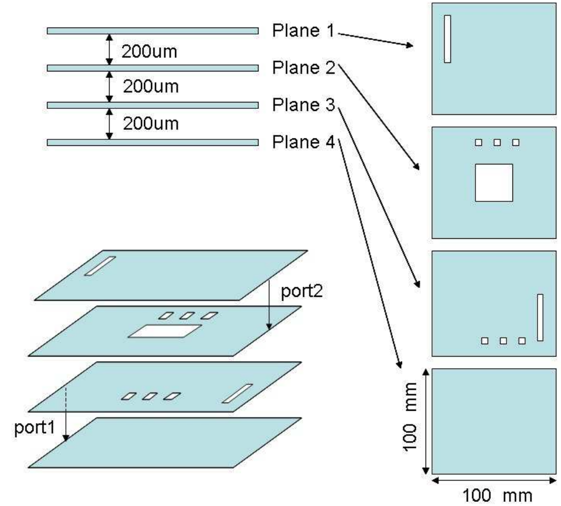

Fig. 4. Four-plane test structure: cross section, location of ports, and top view of each plane.

The integrals in Equations 9 - 10 are a special case of the general formula

$$I = \int\int_{\Omega} L_1^a L_2^b L_3^c dL_1 dL_2 = \frac{a!b!c!}{(a+b+c+2)!} \tag{15}$$

where a, b and c are integer powers. Therefore, substituting $a = 2, b = 0, c = 0$ when $i = j$ and $a = 1, b = 1, c = 0$ when $i \neq j$,

$$m_{i,j} = \frac{-j\omega\varepsilon}{d}\frac{\triangle}{12}(1 + \delta_{i,j}) \tag{16}$$

where $\delta_{i,j}$ is the Kronecker delta function. Using $a = 1, b = 0, c = 0$,

$$f_i = J_z \frac{\triangle}{3} \tag{17}$$

B. Equivalent Circuit

$\overline{\overline{\mathbf{K}}}$ and $\overline{\overline{\mathbf{M}}}$ represent the admittance matrices of frequency-independant inductive and capacitive components, respectively. Specifically, $\overline{\overline{\mathbf{K}}}$ represents inductors connected between triangle vertices (i.e., along the triangle edges), and $\overline{\overline{\mathbf{M}}}$ represents capacitors connected between triangle vertices and to ground, as shown in Figure 3.

This can be shown by evaluating one row of the 3×3 local matrix corresponding to one triangle For example, the sum of the first row of this matrix is:

$$S = \sum_{j=1}^{3} \frac{b_1 b_j + c_1 c_j}{4\triangle} \frac{j}{\omega\mu d}$$

Consider the $b_1 b_j$ term for $j = 1, 2, 3$.

$$b_1^2 = (y_2 - y_3)^2 \text{ for } i = j = 1$$
$$b_1 b_2 = (y_2 - y_3)(y_3 - y_1) \text{ for } i = 1, j = 2$$
$$b_1 b_3 = (y_2 - y_3)(y_1 - y_2) \text{ for } i = 1, j = 3$$
$$\therefore b_1^2 + b_1 b_2 + b_1 b_3 = 0 \tag{18}$$
$$\text{Similarly, } c_1^2 + c_1 c_2 + c_1 c_3 = 0 \tag{19}$$

It can be shown that the other rows of the 3×3 local matrix also sum to zero. This implies that the rows (and by symmetry, the columns) of $\overline{\overline{\mathbf{K}}}$ sum to zero. This corresponds to circuit elements (in this case, inductances) connected between the triangle vertices, with no element to system ground. On the contrary, the row and column sums of $\overline{\overline{\mathbf{M}}}$ do not vanish, indicating capacitances to ground in addition to capacitive elements along edges.

Hence, the equivalent circuit for the single plane-pair case can be represented by the admittance matrix $\overline{\overline{\mathbf{Y}}}$, where $\overline{\overline{\mathbf{Y}}} = \overline{\overline{\mathbf{K}}} + \overline{\overline{\mathbf{M}}}$. This matrix is sparse and the solution to Equation (7) can be obtained using standard linear equation solvers. The ability to obtain an equivalent circuit enables the extension of the method to multiple plane pair geometries, without the need for using 3D-mesh elements (i.e. tetrahedral or hexahedral).

III. Formulation: Multiple Plane-Pairs

A. Meshing

As in the single plane-pair case, a triangular mesh is applied to each metal layer. As will be explained, the multi-layer formulation requires that the location of the mesh nodes be the same on every layer. This is done by flattening or collapsing the features on each metal layer on to one layer, on which triangulation is performed to obtain the mesh. The mesh thus obtained is used to discretize all layers. This is best explained using an example.

Authorized licensed use limited to: Georgia Institute of Technology. Downloaded on August 26, 2009 at 14:46 from IEEE Xplore. Restrictions apply.

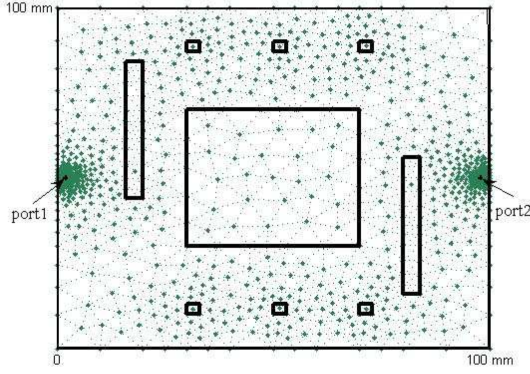

Fig. 5. Top view of the meshed planes.

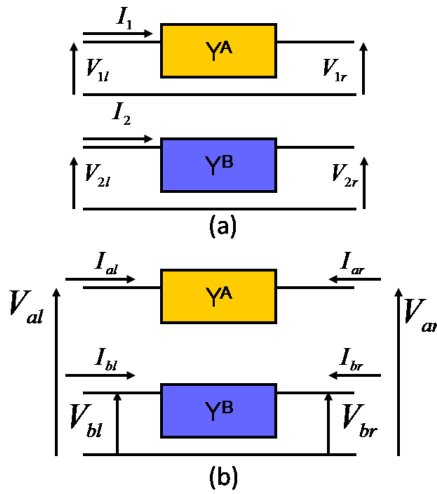

Fig. 6. (a) Two-port networks with separate references (b) Combined four-port network with common reference.

A four-layer structure containing apertures in each layer is shown in Figure 4. When all the features on the multiple layers is flattened onto one layer, the resulting 2D shape contains the outlines of the planes and all apertures. In Figure 5, this 2D shape with a triangular mesh is shown. This mesh can describe the geometrical features (polygon vertices and edges) in any of the layers. The method to obtain the admittance matrix for multiple plane-pair structures is described next.

B. Solid Planes without Apertures

In Section II, the procedure to obtain an equivalent circuit for two-layer geometries with a common ground reference node has been described. For a multiple plane-pair structure containing more than two layers, it is possible to construct an equivalent circuit for each plane-pair. However, the equivalent circuit of different plane pairs assign their respective ground reference node to different layers. Therefore, to obtain the model for the multi-layered plane requires shifting the different reference nodes to one common ground.

This shifting of ground reference nodes can be done using indefinite admittance matrices [11]. This is illustrated, without loss of generality, by using two-port networks with separate ground references, as shown in Figure 6(a). The four-port admittance matrix for the system with the common reference node can be derived as follows:

$$Y_{11}^A V_{1l} + Y_{12}^A V_{1r} = I_1 \quad (20)$$
$$Y_{11}^B V_{2l} + Y_{12}^B V_{2r} = I_2 \quad (21)$$

By noticing that

$$I_{bl} = I_2 - I_1, I_{al} = I_1,$$
$$V_{1l} = V_{al} - V_{bl}, V_{1r} = V_{ar} - V_{br},$$
$$V_{2l} = V_{bl} \text{ and } V_{2r} = V_{br},$$

it is possible to write one row of the admittance matrix of the combined four-port.

$$Y_{11}^A (V_{al} - V_{bl}) + Y_{12}^A (V_{ar} - V_{br}) = I_{al} \quad (22)$$

A similar approach can be used to obtain the complete system in the following form:

$$\begin{pmatrix} Y^A & -Y^A \\ -Y^A & Y^A + Y^B \end{pmatrix} \begin{pmatrix} V_{al} \\ V_{ar} \\ V_{bl} \\ V_{br} \end{pmatrix} = \begin{pmatrix} I_{al} \\ I_{ar} \\ I_{bl} \\ I_{br} \end{pmatrix} \quad (23)$$

For an $M + 1$-layer (M plane-pair) package with solid power/ground planes on each layer, the system matrix, $\overline{\overline{\mathrm{Y}}}$, is obtained as a simple extension of Equation 23.

$$\overline{\overline{\mathrm{Y}}} = \begin{pmatrix} \overline{\overline{\mathrm{Y_1}}} & -\overline{\overline{\mathrm{Y_1}}} & & & \\ -\overline{\overline{\mathrm{Y_1}}} & \overline{\overline{\mathrm{Y_1}}} + \overline{\overline{\mathrm{Y_2}}} & -\overline{\overline{\mathrm{Y_2}}} & & \\ & \ddots & \ddots & \ddots & \\ & & & & -\overline{\overline{\mathrm{Y_{M-1}}}} \\ & & & -\overline{\overline{\mathrm{Y_{M-1}}}} & \overline{\overline{\mathrm{Y_{M-1}}}} + \overline{\overline{\mathrm{Y_M}}} \end{pmatrix} \quad (24)$$

, where $\overline{\overline{\mathrm{Y_i}}}$, $i = 1, 2, \ldots, M$ are admittance matrices obtained for the ith plane-pair counting from the top of the stack.

C. Inclusion of Apertures

Without apertures, the problem domain is simply a rectangle. In a more complex case with apertures, the flattened problem domain can be decomposed into a number of sub-domains, containing the solid metal planes and the apertures. To further explain this concept, an $M + 1$-layer package with an arbitrary number of apertures on each layer can be flattened into a rectangular problem domain containing N sub-domains. Each of these sub-domains represents one aperture or many overlapping apertures.

Thus, while adding the contributions of each layer i, $i = 1, 2, \ldots, M$, to the admittance matrix, the following cases are considered. As before, $i = 1$ is the top-most layer.

1) **Sub-domains $j_1, j_2, \ldots, j_P$ correspond to no apertures on layers i and $i + 1$:** This case is handled

Authorized licensed use limited to: Georgia Institute of Technology. Downloaded on August 26, 2009 at 14:46 from IEEE Xplore. Restrictions apply.

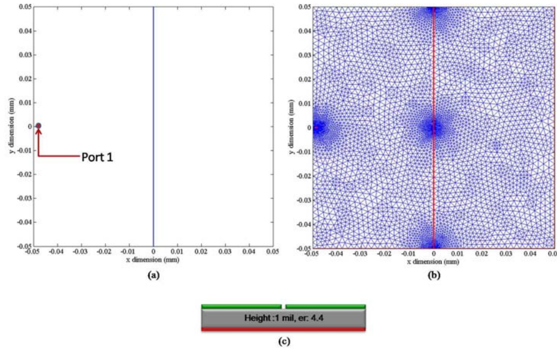

Fig. 7. (a)Geometry of split-plane structure (b) Mesh (c) Cross-section.

as in the previous sub-section. The contributions of the sub-domains $j_1, j_2, \ldots, j_P$ are added to $\overline{\overline{\mathrm{Y_i}}}$ without alteration.

2) **Sub-domains $k_1, k_2, \ldots, k_Q$ correspond to apertures on layer i:** The contributions of sub-domains $k_1, k_2, \ldots, k_P$ are removed from $\overline{\overline{\mathrm{Y_i}}}$.

3) **Sub-domains $l_1, l_2, \ldots, l_R$ correspond to apertures on layers $i+1, i+2, \ldots, i+X$:** The contributions of sub-domains $l_1, l_2, \ldots, l_R$ are removed from $\overline{\overline{\mathrm{Y_i}}}$. Create admittance matrix M containing the contributions of the excluded sub-domains, with reference to corresponding nodes in layer $X+1$.

IV. Results

The critical problem with finite difference methods such as MFDM is that in the presence of small features, the mesh becomes dense, as a result of which the number of unknowns in the system can be large. An example to illustrate this is a single plane-pair test case. The lower metal layer is a solid ground plane, while the top layer, of dimensions 100mm $\times$ 100mm contains a 0.2mm slot, dividing it into two 100mm$\times$49.9mm islands. The geometry of the structure, the mesh, and the cross-section are shown in Figures 7(a), 7(b) and 7(c) respectively. The only port in the structure is placed on one of the power islands. The slot width (0.2 mm) is large enough when compared to the dielectric height (1 mil) that gap coupling can be ignored. As a consequence of the Delaunay mesh generation algorithm that has been used, the mesh is denser around small features and coarse elsewhere.

The structure was simulated with MFEM, as well as MFDM. All simulations were performed on an Intel Core2 Duo 2.2 GHz workstation with 2.0 GB RAM. The impedance at Port 1, Z_{11} is shown in Figure 8, and there is good agreement between MFEM and MFDM. A summary of the computational requirements are listed in Table I.

To validate MFEM, two test cases have been considered. The following test cases were designed to demonstrate the capability to model vertical coupling through apertures in the metal planes.

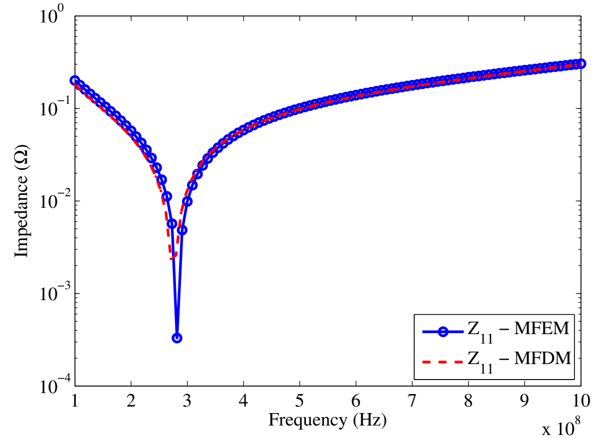

Fig. 8. Self Impedance Z_{11}

TABLE I
SUMMARY OF RESULTS.

Method	Unknowns	Time / Freq Pt.	Code	MFEM Speed-up
MFEM	1,439	0.250 s	MATLAB	-
MFDM	250,000	10 s	C++	40X

The geometries of the first test case is shown in Figures 9, along with the port locations.

Ideally, if the metal-layers were all solid and contained no holes or apertures, then there will be no coupling between the ports, at the frequencies of interest. This is due to the fact that the field penetration depth reduces with frequency. The skin-depth can be expressed as

$$\delta_s = \sqrt{\frac{1}{\pi f \mu \sigma}} \tag{25}$$

, where f is the frequency of operation, μ is the permittivity of the medium and σ is the conductivity of the metallization. At 100 MHz, for copper metallization, the skin-depth is approximately 7 μm (and 2 μm at 1 GHz). In these test cases, the copper used was 30 μm thick. Hence, field penetration will not play a major role over the frequencies of interest ($>$ 100 MHz).

However, from the insertion loss results shown in Figures

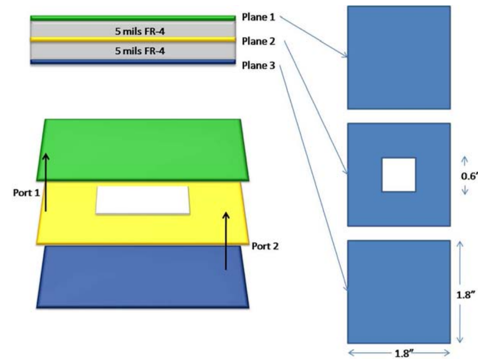

Fig. 9. Test vehicle 1 (a) Geometry (b) Stack cross-section.

Authorized licensed use limited to: Georgia Institute of Technology. Downloaded on August 26, 2009 at 14:46 from IEEE Xplore. Restrictions apply.

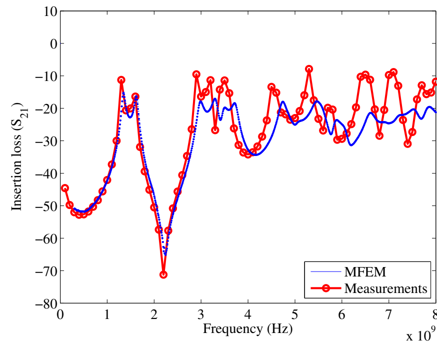

Fig. 10. Insertion loss for structure in Figure 9.

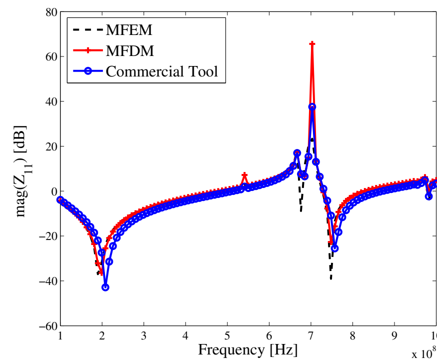

Fig. 11. Magnitude of Self Impedance (Z_{11}).

10, there is significant coupling between ports. This is due to aperture coupling. Also, the results from MFEM correlate well with measurements.

The second test case is the four-layer structure that was previously used to explain the meshing scheme, with plane dimensions of 100mm × 100mm. The differences in dimensions of each aperture was maximized to emphasize the meshing scheme employed by MFEM. Hence, the largest aperture size was 40×40 mm and the smallest was 3×3 mm. The minimum aperture size was chosen such that it still influenced the response of the structure at the maximum simulation frequency of 1GHz. Two ports are placed between the bottom plane (ground) and the second plane, and between the third plane and the top plane, respectively, as shown in Figure 4. The dielectric is FR-4 with $\epsilon_r = 4.4$.

The structure was simulated with MFEM, which has been implemented using MATLAB, and the results were compared with MFDM [3] and a commercial power integrity simulator. The commercial tool performs 2.5-D simulation using FEM. The self and transfer impedance results have been plotted in Figures 11 and 12. As can be seen from the results, there is good correlation between MFEM and the others methods. A summary of the results with timing information and implementation details has been provided in Table II.

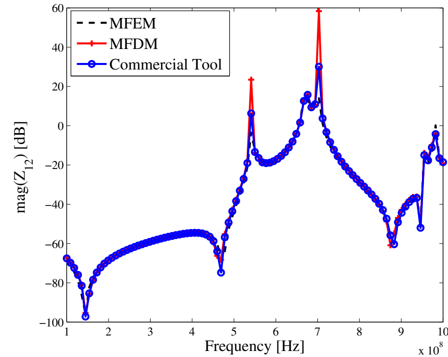

Fig. 12. Magnitude of the transfer impedance (Z_{12}).

TABLE II
SUMMARY OF RESULTS FOR STRUCTURE IN FIGURE 4

Method	Unknowns	Time / 100 Freq Pt.	Code	MFEM Speed-up
MFEM	3,594	35 s	MATLAB	-
MFDM	122,411	560 s	C++	16X
Comm. tool	71,204	200 s	Unknown	5.5X

V. Conclusions

In this paper, a novel modeling method to obtain the frequency response of multi-layer package power/ground planes has been proposed. This method, MFEM, results in a system which is sparse, while only applying a 2D triangular mesh on the metal surface. Thus, MFEM has been shown to require significantly fewer unknowns and still provide accuracy comparable with other simulation methods.

References

[1] M. Swaminathan and A. E. Engin, *Power Integrity Modeling and Design for Semiconductors and Systems*. Prentice Hall, 2007.
[2] A. E. Engin, K. Bharath, and M. Swaminathan, “Multilayered finite-difference method (m-fdm) for modeling of package and printed circuit board planes,” *IEEE Trans. Electromag. Compat.*, vol. 49, no. 2, pp. 441–447, May 2007.
[3] K. Bharath, E. Engin, M.Swaminathan, K. Uriu, and T. Yamada, “Computationally efficient power integrity simulation for system-on-package applications,” in *Proc. of 44th Design Automation Conference*, July 2007, pp. 612 – 617.
[4] K.-B. Wu, G.-H. Shiue, W.-D. Guo, C.-M. Lin, and R.-B. Wu, “Delaunay-voronoi modeling of power-ground planes with source port correction,” *IEEE Trans. on Adv. Packaging*, vol. 31, no. 2, pp. 303–310, May 2008.
[5] C. Guo and T. H. Hubing, “Circuit models for power bus structures on printed circuit boards using a hybrid fem-spice method,” *IEEE Trans. on Adv. Packaging*, vol. 29, no. 3, pp. 441–447, August 2006.
[6] K. Bharath and M. Swaminathan, “Multi-layer finite element method (mfem) for the modeling of package power/ground planes,” Georgia Tech invention disclosure 4719, January 2009.
[7] T. Okoshi and T. Miyoshi, “The planar circuit - an approach to microwave integrated circuitry,” *IEEE Trans. Microwave Theory Tech.*, vol. MTT-20, pp. 245–252, April 1972.
[8] E. T. Itoh, *Numerical Techniques for Microwave and Millimeter-Wave Passive Structures*. John Wiley, 1989.
[9] P. P. Silvester and R. L. Ferrari, *Finite Elements for Electrical Engineers*. Cambridge University Press, 1983.
[10] A. F. Peterson, S. L. Ray, and R. Mittra, *Computational Methods for Electromagnetics*. IEEE Press, 1998.
[11] J. A. Dobrowolski, *Introduction to Computer Methods for Microwave Circuit Analysis and Design*. Artech House, 1991.

Authorized licensed use limited to: Georgia Institute of Technology. Downloaded on August 26, 2009 at 14:46 from IEEE Xplore. Restrictions apply.